FISEVIER

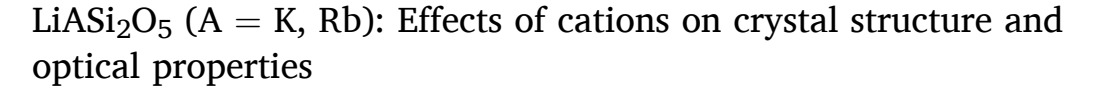
Contents lists available at ScienceDirect

Optical Materials

journal homepage: www.elsevier.com/locate/optmat



Research Article



Jun Sun a,b, Bo Ran b, Ping Hu b, Zhaofeng Wu b, Ming-Hsien Lee, Haiming Duan b, **

- ^a Xinjiang Key Laboratory of Solid-State Physics and Devices, Urumgi, Xinjiang, 830046, China
- ^b School of Physics Science and Technology, Xinjiang University, Urumqi, Xinjiang, 830046, China
- ^c Department of Physics, Tamkang University, New Taipei City, 25137, Taiwan

ARTICLE INFO

Keywords: Tetrahedral units Cation effect Nonlinear optical crystal Phase matching First principles calculation

ABSTRACT

Tetrahedral basic building units are important for the design of new nonlinear optical materials. In this paper, two alkali metal silicates have been reported to have differentiated symmetry and optical properties. LiKSi₂O₅ crystallizes in the monoclinic system of $P2_1$ with the ultraviolet cutoff of 255 nm; LiRbSi₂O₅ crystallizes in the orthorhombic system of $Pca2_1$ with the ultraviolet cutoff of 240 nm. The calculation results show that the second harmonic generation coefficients and the wavelengths of phase matching for LiKSi₂O₅ are $d_{16} = 0.30$ pm/V and 585 nm, while that for LiRbSi₂O₅ are $d_{24} = 0.38$ pm/V and 446 nm, respectively. Hence, the different radii of cations lead to different coordination environments, which will affect the connection styles further influences the symmetries and optical properties of the compounds. It is confirmed that simple ion substitution can change the optical properties, which provides a feasible way for the modulation of nonlinear optical property.

1. Introduction

Nonlinear optical (NLO) materials capable of efficiently expanding the wavelengths of solid-state laser from the deep ultraviolet (deep-UV) (<200 nm) to the infrared (IR) region (~20 μ m) play a crucial role in modern laser science and technology [1–14]. In the past few decades, great efforts have been made in the design and synthesis of new NLO materials with high performance, especially for deep-UV/UV NLO materials. Up to now, the research interests are dominantly focused on borates and phosphates [1,11,15–18], such as β -BaB₂O₄ (β -BBO) [19], KBe₂BO₃F₂ (KBBF) [20], LiB₃O₅ (LBO) [21], Sr₂Be₂B₂O₇ (SBBO) [22], K₃B₆O₁₀Cl [23], Ba₃P₃O₁₀X (X = Cl, Br) [24], LiCs₂PO₄ [25,26], NH₄Be₂BO₃F₂ [27], C(NH₂)₃BF₄ [28]. Among them, the KBBF- and SBBO-like compounds have been widely considered as the most promising deep-UV NLO materials.

Apart from borates and phosphates containing $[BO_4]$ and $[PO_4]$ anionic groups, $[SiO_4]$ tetrahedra are also considered as optional anionic groups. According to the anionic group theory [29-31], non- π conjugated tetrahedra groups, such as the hyperpolarizability of $[BO_4]$, $[PO_4]$, $[SiO_4]$, etc. are one order smaller than the planar $[BO_3]$ groups for the microscopic second harmonic generation (SHG) effect generation.

Therefore, the method for enhancing SHG responses of these materials is to make the anionic groups align in the same direction with high density or condense those non- π conjugated tetrahedra groups that may help to increase the distortion of tetrahedra. As we known, silicates have the most abundant constituents in the earth's crust, and α -SiO₂ is also the first NLO crystal which allow the observation of the frequency doubling effect. As a result, the silicate system has the potential to be applied in the field of NLO. Li₂K₄[(TiO)Si₄O₁₂] and Li₂Rb₄[(TiO)Si₄O₁₂], for instance, have efficiencies of about 4.5 times KH₂PO₄ (KDP) with a moderate birefringence and resistant laser damage [32]. Li₂BaSiO₄ is demonstrated to have a significant SHG response, 2.8 × KDP, with edge-sharing [LiO₄]-[SiO₄] tetrahedra [33]. By adding Pb²⁺ with a stereochemically active lone pair, PbSrSiO₄ with 5.8 times KDP was produced [34]. The SHG intensities of KNbSi₂O₇, PbZnSiO₄, and Na₂TiSiO₅ are 6.7, 2.9, and 2.8 times that of KDP [35]. The silicates with diverse types of anion groups have come into our research scope. And, there are diverse types of anion groups in silicates [33,36–39], such as $[SiO_4]$, $[Si_2O_7]$, $[Si_3O_9]$, $[Si_4O_{12}]$, and $[Si_6O_{18}]$. Furthermore, the Siatom is normally bound to four O atoms to form a [SiO₄] tetrahedron, whereas the configuration is widely accepted to be useful for facilitating a short absorption edge. Thus, we expected that the silicates may be also

^{*} Corresponding author.Xinjiang Key Laboratory of Solid-State Physics and Devices, Urumqi, Xinjiang, 830046, China.

^{**} Corresponding author. Xinjiang Key Laboratory of Solid-State Physics and Devices, Urumqi, Xinjiang, 830046, China. *E-mail addresses:* wuzf@xju.edu.cn (Z. Wu), dhm@xju.edu.cn (H. Duan).

Table 1 Crystal data and structural refinement for LiASi $_2O_5$ (A = K, Rb).

Empirical formula	$LiKSi_2O_5$	$\rm LiRbSi_2O_5$
Formula weight	182.22	228.59
Temperature (K)	293(2)	302(2)
Wavelength (Å)	0.71073	0.71073
Crystal system	Monoclinic	Orthorhombic
Space group	P2 ₁ (No. 4)	Pca2 ₁ (No. 29)
Unit cell dimensions (Å,	a = 6.0009(7)	a = 16.4795(14)
°)	b = 4.8082(5)	b = 6.0599(6)
	c = 8.1967(9)	c = 4.8700(4)
	$\beta = 93.579(4)$	
Volume (ų)	236.04(5)	486.34(7)
Z, Density (g/cm ³)	2, 2.564	4, 3.122
Absorption coefficient (mm ⁻¹)	1.555	10.597
F (000)	180	432
Theta range for data collection (°)	2.49 to 27.54	2.47 to 29.71
Limiting indices	$-7 \le h \le 7, -6 \le k \le 6,$	$-21 \le h \le 22, -8 \le k \le 8,$
	$-10 \leq l \leq 10$	$-5 \le l \le 6$
Reflections collected/	3894/1031 [R(int) =	2930/1202 [R(int) =
unique	0.0813]	0.0634]
Completeness (%)	99.2	98.7
Data/restraints/ parameters	1031/1/84	1202/1/82
Goodness-of-fit on F^2	1.187	1.059
Final R indices $[F_o^2>2\sigma]$	$R_1 = 0.0437, wR_2 =$	$R_1 = 0.0436, wR_2 =$
(F_o^2)] ^a	0.0745	0.0799
R indices (all data) ^a	$R_1 = 0.0587, wR_2 =$	$R_1 = 0.0701, wR_2 =$
	0.0777	0.0907
Largest diff. peak and hole (e- \mathring{A}^3)	0.532 and -0.602	0.660 and -0.713

 $^{^{}a}\ R_{1}=\Sigma\big|\big|F_{o}\big|\cdot\big|F_{c}\big|\big|/\Sigma\big|F_{o}\big|\ \ \text{and}\ \ wR_{2}=\big[\Sigma w(F_{o}^{2}-F_{c}^{2})2/\Sigma w\ F_{o}^{4}\big]^{1/2}\ \ \text{for}\ F_{o}^{2}>2\sigma(F_{o}^{2}).$

potential candidates for NLO applications. To date, silicates as NLO materials are rarely reported.

Herein, in this paper, we expect to synthesize the two silicates by introducing the alkaline cations without d-d or f-f electron transitions resulting in the wide transparent regions. Activated by this, a new NLO material LiRbSi $_2O_5$ was synthesized. And, LiKSi $_2O_5$ was also synthesized successfully which was determined by de Jong et al. firstly [40]. In addition, Du et al. investigated a series of alkali silicates by using computer modeling techniques to study the size effect of alkali ions including LiKSi $_2O_5$, and predicting the structure of LiRbSi $_2O_5$ in the monoclinic space group (a = 6.53, b = 5.05, c = 17.04, β = 95.72°) which is different from what we have been synthesized in this paper [41, 42]. Herein, the synthesis, structural analysis, thermal stability, birefringence behavior, and the structure-property relationship of LiASi $_2O_5$ (A = K, Rb) were reported.

2. Experimental section

2.1. Reagents

 $\rm Li_2CO_3,\,K_2CO_3,\,Rb_2CO_3,\,and\,SiO_2$ were used as reagents. All of them are analytical grade and purchased without further purification.

2.2. Synthesis

Crystals of LiASi $_2$ O $_5$ (A = K, Rb) were grown from the traditional high-temperature solid-state reaction technique. The Li $_2$ CO $_3$, A $_2$ CO $_3$ (A = K, Rb), and SiO $_2$ reagents in the molar ratio of 1:1:2 were mixed and put into platinum crucibles, respectively, which were heated to 950 °C and held at this temperature for 10 h to homogenize the solution. Then the temperature was reduced to 700 °C at a rate of 1 °C/h, then to 500 °C at a rate of 2 °C/h, and finally cooled to room temperature at a rate of 10 °C/h. During the slow cooling processes, the small single crystals of LiASi $_2$ O $_5$ (A = K, Rb) were obtained.

2.3. Solid-state synthesis

Polycrystalline samples of LiASi $_2O_5$ (A = K, Rb) were obtained by employing solid-state techniques. Li $_2CO_3$, A $_2CO_3$ (A = K, Rb), and SiO $_2$, according to a ratio of 1:1:2, were gradually heated to the appropriate temperatures (about 750 °C) with several intermediate grindings which were maintained at the selected temperatures for 7 days to ensure complete reactions. The purities of the polycrystalline sample were confirmed by employing powder X-ray diffraction (PXRD) measurements.

2.4. Single-crystal X-ray diffraction

The single-crystal X-ray diffraction data were collected at 296 K on a Bruker APEX II CCD diffractometer equipped with a monochromatic Mo $K\alpha$ radiation source ($\lambda=0.71073$ Å). The SAINT program was employed to carry out the data integration, cell refinement, and absorption corrections [43]. The crystal structures were solved via the SHELXTL crystallographic software package [44]. The structures were checked with the PLATON program for promoting symmetry elements [45]. Crystallographic data and structure refinement information of LiASi $_2O_5$ (A = K, Rb) are given in Table 1. The atomic coordinates, isotropic thermal parameters, the values of the bond valence sum (BVS), and the interatomic bond lengths of LiASi $_2O_5$ (A = K, Rb) are listed in Tables S1–S4.

2.5. Powder X-ray diffraction

The powder X-ray diffraction (PXRD) data were recorded by using a Bruker D2 PHASER diffractometer equipped with a monochromatized Cu K α radiation source ($\lambda=1.5418$ Å) at room temperature. The PXRD patterns for LiASi₂O₅ (A = K, Rb) are plotted in Fig. S1, which exhibited the experimental patterns fit well with the calculated ones.

2.6. Infrared spectroscopy

Infrared (IR) spectra were measured using a Shimadzu IR Affinity-1 Fourier transform IR spectrometer in the range from 400 to 4000 cm⁻¹ with a resolution of 2 cm⁻¹ at room temperature. KBr was used as the reference pellet, and the samples were mixed thoroughly with it.

2.7. UV-Vis-NIR diffuse reflectance spectroscopy

The UV-vis-NIR diffuse reflectance spectra for LiASi $_2$ O $_5$ (A = K, Rb) were measured on a Shimadzu SolidSpec-3700DUV spectrophotometer with a wavelength range from 180 to 2600 nm at room temperature. The reflectance spectra were converted to absorption based on the Kubelka-Munk function: $F(R) = (1-R)^2/2R = K/S$ (R = reflectance; K = absorption; S = scattering).

2.8. Thermal analysis

Thermal gravimetric analyses (TG) and differential scanning calorimetry (DSC) were performed on a NETZSCH STA 449F3 simultaneous analyzer at a rate of 5 $^{\circ}$ C/min under flowing nitrogen gas.

2.9. Theoretical calculations

The band structures, the partial density of states (PDOS), and birefringence of LiASi $_2O_5$ (A = K, Rb) were calculated by utilizing the CASTEP program [46,47]. The exchange-correlation functional was adopted by the generalized gradient approximation (GGA) with the Perdew-Burke-Ernzerhof (PBE) functional [47]. Under the norm-conserving pseudopotential (NCP) [48,49], the following orbital electrons were treated as valence electrons: Li, $2s^1$; K, $3s^23p^64s^1$; Rb, $4s^24p^65s^1$; Si, $3s^23p^2$; O, $2s^22p^4$. The energy cutoffs of the plane-wave

J. Sun et al. Optical Materials 148 (2024) 114815

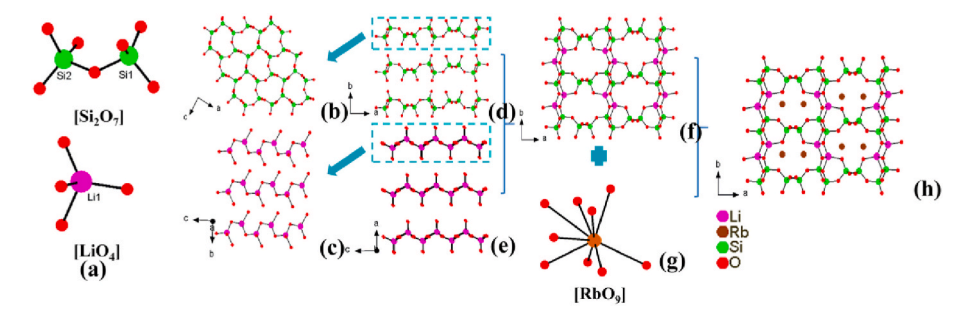


Fig. 1. The 3D structure of LiRbSi₂O₅. (a) The [LiO₄] tetrahedron and the [Si₂O₇] unit; (b) The single layer made up of the [Si₂O₇] units viewed from the b axis; (c) The lines formed by [LiO₄] tetrahedra seen from the a-axis; (d) The Si-O layers seen from the c axis; (e) The Li-O chains viewed from the b axis; (f) The 3D framework formed by Si-O layers and Li-O chains; (g) The [RbO₉] polyhedron; (h) The 3D structure of LiRbSi₂O₅.

basis were set at 830 eV for the two compounds and the k-point grid sampling in the Monkhorst-Pack scheme were set at $4\times5\times3$ for LiK-Si₂O₅, $2\times4\times5$ for LiRbSi₂O₅, respectively, with a separation of 0.04 Å⁻¹ in the Brillouin zone. The refractive indices and the birefringence Δn can be acquired by electronic structures and Kramers-Kronig transformation [50]. The calculation of optical properties was scissor-corrected by the difference between the GGA-PBE and experimental energy gaps. The SHG coefficients are also obtained by using the band structures calculated by the CASTEP package. And, the second-order nonlinear susceptibilities at the limit of zero frequency, $\chi^{(2)}_{\alpha\beta\gamma}(0)$, can be expressed as the sum of the contribution of the virtual-electron (VE) processes and the virtual-hole (VH) processes: [51, 521.

$$\chi_{\alpha\beta\gamma}^{(2)} = \chi_{\alpha\beta\gamma}^{(2)} \text{ (VE)} + \chi_{\alpha\beta\gamma}^{(2)} \text{ (VH)}$$

$$\chi_{\alpha\beta\gamma}^{(2)} \text{ (VE)} = \frac{e^3}{2\hbar m^3} \sum_{vcc} \int \frac{d^3k}{4\pi^3} P(\alpha\beta\gamma) Im \left[P_{cv}^{\alpha} P_{cc}^{\beta} P_{cv}^{\gamma} \right] \left(\frac{1}{\omega_{cv}^3 \omega_{vc}^2} + \frac{2}{\omega_{vc}^4 \omega_{cv}} \right)$$

$$\chi^{(2)}_{\alpha\beta\gamma}(\mathrm{VH}) = \frac{e^3}{2\hbar m^3} \sum_{vvc} \int \frac{d^3k}{4\pi^3} P(\alpha\beta\gamma) Im \left[P^{\alpha}_{vv} P^{\beta}_{cv} P^{\gamma}_{cv} \right] \left(\frac{1}{\omega^3_{cv} \omega^2_{vc}} + \frac{2}{\omega^4_{vc} \omega_{cv}} \right)$$

Here, α , β , and γ subscripts show Cartesian components while ν , ν' , and c, c' denote the valence bands (VBs) and conduction bands (CBs). $P(\alpha\beta\gamma)$, ω_{ij} , and P^{α}_{ij} denote full permutation, band energy difference, and momentum matrix elements, respectively.

3. Results and discussion

Crystals of LiASi $_2$ O $_5$ (A = K, Rb) were grown from the traditional high-temperature solid-state reaction technique. And, terminal stabilities of LiASi $_2$ O $_5$ (A = K, Rb) were evaluated by TG-DSC which are shown in Fig. S1. There is only one endothermic peak at 817 °C for LiKSi $_2$ O $_5$ and 875 °C for LiRbSi $_2$ O $_5$ on the heating curves of their DSC curves, respectively. The sole endothermic peaks of them should be corresponding to the melt of the compounds. While there are no peaks on the cooling plots, which is caused by the high viscosity of the silicate systems. From the TG curves of the two compounds, we can find that the

weight loss of LiRbSi $_2O_5$ is more than that of LiKSi $_2O_5$. To further know their thermal behaviors, their polycrystalline samples were placed in Pt crucibles with heating over the melting temperature and maintained at the selected temperature for 48 h, then cooled the temperature to recrystallize. As shown in Fig. S2, there are some differences in the curves between the before and after recrystallizing for the two compounds. And, the superfluous peaks of the curves in LiKSi $_2O_5$ are less than that in LiRbSi $_2O_5$. The superfluous peaks which are marked with red five-pointed stars (Fig. S2) are belonging to that of Li $_2$ Si $_2O_3$ (PDF NO. 29-0829). So, when the two compounds were heated over the melting temperature or with a long holding time would cause a small amount of volatilization of K or Rb atoms. And, the volatilization of the K atom is less than that of the Rb atom which fits well with the weight loss of LiKSi $_2O_5$ is less than that of LiRbSi $_2O_5$ on the TG curves.

 ${\rm LiASi_2O_5}$ (A = K, Rb) have similar stoichiometries but crystallize in different crystal systems (Table 1). ${\rm LiKSi_2O_5}$ crystallizes in the monoclinic system of $P2_1$, whereas ${\rm LiRbSi_2O_5}$ in the orthorhombic system of $Pca2_1$.

The structures of LiASi₂O₅ (A = K, Rb) are shown in Fig. 1 and S3. In the asymmetric units, there is one Li atom, one A atom, two Si atoms, and five O atoms. LiASi2O5 (A = K, Rb) exhibits a 3D network that consists of Si-O layers and Li-O chains with the A atoms staying in the space (Fig. 1h and S3a). All Si atoms are coordinated by four O atoms to form [SiO₄] tetrahedra, and two [SiO₄] tetrahedra compose the [Si₂O₇] units by sharing O atoms (Fig. 1a and S3c), then the [Si₂O₇] units form the Si-O single layers (Fig. 1b and d, and S3c). All of the Li atoms also form tetrahedra (Fig. 1a and S3d), and the neighboring [LiO₄] tetrahedra further compose one-dimensional (1D) endless [LiO₃] chains (Fig. 1c and e, and S3d). The Li-O and Si-O bond lengths range from 1.905(12) to 2.189(13) Å and from 1.571(4) to 1.654(5) Å in LiRbSi₂O₅, from 1.894(10) to 2.107(8) Å and from 1.562(3) to 1.647(4) Å in LiK-Si₂O₅, respectively. The three-dimensional (3D) framework (Fig. 1f and S3b) of LiASi₂O₅ (A = K, Rb) can be regarded as formed by 1D Li-O chains and two-dimensional (2D) Si-O layers with one Rb⁺/K⁺ cation balancing the charge of this anionic framework (Fig. 1h and S3a). The Rb⁺ and K⁺ cations are both nine-coordinated with Rb/K-O bond lengths ranging from 2.850(8) to 3.453(5) Å, from 2.739(4) to 3.251(3) Å, respectively. The bond valence sums (BVSs) calculations resulted in the

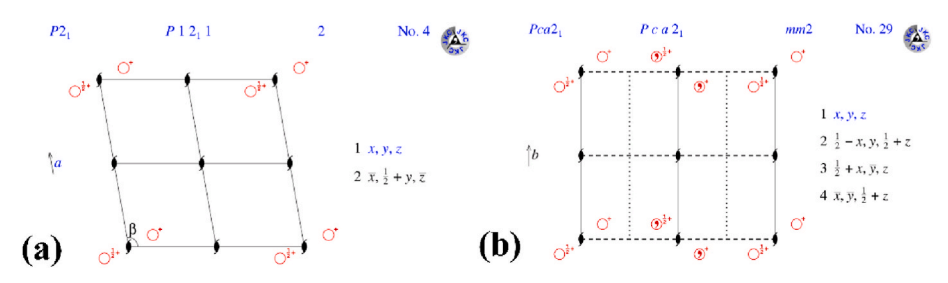


Fig. 2. (a) The space group of $P2_1$. (b) The space group of $Pca2_1$.

Fig. 3. UV-vis-NIR spectra (a) and Infrared spectra (b) of LiASi₂O₅ (A = K, Rb).

values of 1.04 for Li $^+$, 1.02 for Rb $^+$, 0.84 for K $^+$, 4.01-4.04 for Si $^{4+}$, and 1.92-2.11 for O 2 (Tables S2 and S4).

Interestingly, LiASi₂O₅ (A = K, Rb) exhibit similar stoichiometries which crystallize in different crystal systems. The symmetry operations of the two space groups are demonstrated in Fig. 2. The Symmetry of $P2_1$ (Fig. 2a), LiKSi₂O₅, is lower than of $Pca2_1$ (Fig. 2b), LiRbSi₂O₅, mainly due to the $\beta \neq 90^\circ$ in $P2_1$. And, the symmetry operations of the two space groups are different, where $P2_1$ performs inversion and translation operations, while $Pca2_1$ also has slip operations. In addition, the coordination environment of Li, K/Rb, and Si atoms, the bond length range of Li-O, A-O, Si-O, and the bond angle range of O-Li-O, O-A-O, O-Si-O are displayed in Table S5. Then we will divide the discussion into two parts-anionic frameworks and the coordination environments of cations.

The comments of anionic frameworks are as follows: (1) The topological structures are similar which simplifies the [LiO₄] and [SiO₄] tetrahedra as spots (Figs. S4a and S4b) of the 3D framework in the two compounds. The symmetry of LiRbSi₂O₅ is higher than that of LiKSi₂O₅; (2) The waved 1D endless Li-O chains are found between the two compounds (Figs. S4c and S4d) and the angles of Li-Li-Li are 98.12° in $LiKSi_2O_5,\ 98.57^\circ$ in $LiRbSi_2O_5,\ respectively,\ which show a small different constant of the contraction of the contra$ ference. What's more, the distances between the adjacent Li-O chains are also considered. The distance in LiKSi₂O₅ is 8.20 Å which is shorter than that in LiRbSi₂O₅ because of the difference in filling cation in channels; (3) The Si-O units both formed the layers in the two compounds (Figs. S4e, S4f, S4g, and S4h). And, the distances between the two Si atoms in adjacent layers (Figs. S4e and S4f) are 6.00 Å in LiK-Si₂O₅, and 6.06 Å in LiRbSi₂O₅, respectively. Amplified the Si-O single layers, they are both formed by 12 Members-Rings (MRs) (Figs. S4i and S4j) which are composed of six [SiO₄] tetrahedra by sharing O atoms. The angles among the SiN-SiN-SiN (N = 1 or 2) which formed the 12-MRs range from 89.35 to 122.47° in LiKSi₂O₅ whereas from 90.09 to 128.47° in LiRbSi₂O₅, respectively. The differences mainly focus on two angles. Firstly, the angle of Si2-Si2-Si1 is 122.47° in LiKSi₂O₅ corresponding to Si1-Si1-Si2 is 128.47° in LiRbSi₂O₅. Secondly, the angle of Si1-Si2-Si2 is 108.36° in LiKSi2O5 corresponding to Si2-Si1-Si1 is 115.85° in LiRbSi₂O₅. The differences in the angles are about 7° between the two angles, respectively.

The anionic frameworks in the two compounds were discussed earlier, then the coordination environments of cations will be discussed. (1) The K and Rb atoms are both nine-coordinated with O atoms in the two structures. And, the bond length range of K-O is shorter than that of Rb-O because of the differences in cation radius. And the bond angle range of O-K-O is from 47.8 to 167.1° narrower than that of O-Rb-O with a range of 37.2-170.00° (Table S5). (2) The K-O units are formed in two different chains along with the *c* and *a*-axis while only one type of chain for Rb-O units is found along the *a*-axis (Figs. S5a and S5b). And, the angles of O5-K1-O2 and O5-K1-O2 are 69.84° and 86.30° along the *c*-axis which correspond to 67.14° and 125.24° for O5-Rb1-O1 and O1-Rb1-O5 along *a*-axis. The angle of O3-K1-O3 which formed the chains along the *a*-axis is 131.69° while the angle of O2-Rb1-O1 is 136.96° (Fig. 5c and d). (3) There are three different types of bond lengths

between the K-K atoms or Rb-Rb atoms, 6.00, 3.88, 5.73 Å or 7.77, 3.84, 5.88 Å, respectively. (4) In the black square frames (marked in Figs. S5a and S5b), the connection types of K-O-K are the same as that of Rb-O-Rb while there are quite differences in the blue square frames. (5) Seen from the other direction, the shorter bond lengths could lead to larger range angles (Figs. S5e and S5f). The angles of K-O-K are ranging from 99.31 to 121.11° which are wider than that of Rb-O-Rb ranging from 101.40 to 117.21° .

In a word, the different radii of cations lead to different coordination environments for all the cations (including bond lengths and bond angles of the cations), which will further affect the connection styles among the cations. Then, when occurring those changes, the anion frameworks will also change which further influences the symmetries of crystal structures.

The UV-vis-NIR spectra of LiASi $_2$ O $_5$ (A = K, Rb) are plotted in Fig. 3a. The transmittance spectrum measurement shows that those UV cut-off edges are about 240-255 nm corresponding to 5.78 eV for LiKSi $_2$ O $_5$, 5.94 eV for LiRbSi $_2$ O $_5$, respectively, which are comparable with other crystals, e.g. Ba $_2$ TiOSi $_2$ O $_7$ (240 nm) [53], Sr $_2$ ZnSi $_2$ O $_7$ (225 nm) [54], Sr $_2$ MgSi $_2$ O $_7$ (220 nm) [54], Li $_2$ MSiO $_4$ (M = Sr, Ba) (<190 nm) [33].

 $LiASi_2O_5$ (A = K, Rb) exhibits similar IR spectra which are depicted in Fig. 3b. As shown in Fig. 3b, the peaks at 633-1099 cm⁻¹ are mainly due to the stretching vibration of [SiO₄] tetrahedra. And, the bands associated with the bending vibration of [SiO₄] groups are located at about 462-574 cm⁻¹. This is proved the existence of [SiO₄] tetrahedra.

Furthermore, the electronic and optical properties of LiASi₂O₅ (A = K, Rb) were calculated by using first-principles calculations [46]. Planewave cutoff was chosen to ensure the total energy convergence is within 0.1 eV/atom. Uniform k-point sampling of Monkhorst-Pack style was made with the grid spacing 0.05 Ang-1. Calculated optical properties has been tested converged user such parameters. Both compounds are indirect band-gaps with calculated band-gaps of 4.473 and 4.805 eV for LiKSi₂O₅ and LiRbSi₂O₅, respectively (Figs. S6a and S6b), which are smaller than experimental values (5.94 eV, 5.78 eV) attributable to the discontinuity of exchange-correlation energy [55]. The partial electronic densities of states (PDOS) are shown in Figures S7c and S7d. For LiKSi2O5, the top of valence bands (VBs) consist almost exclusively of O-2p orbitals with small contributions from Si-3p orbitals, while the bottoms of the conduction bands (CBs) are primarily K-s, Li-2s orbitals with small contributions from Si-3s, O-2p orbitals. For LiRbSi₂O₅, the VBs consist of O-2p and Si-3p orbitals with small amounts from Rb-s, Rb-4p, and Li-2s orbitals, while the CBs are Si-3s, with small amounts from Li-2s, Rb-s, and O-2p orbitals. The obvious differences are found from -5 to 0 eV and near 5 eV. From -5 to 0 eV in LiRbSi₂O₅ is overlapping whereas that is little overlapping in LiKSi2O5, which suggests that there is a strong bond-interaction for Si and O atoms in LiRbSi₂O₅. And thus, near 5 eV, Li 2s and K s orbitals make major contributions in LiKSi₂O₅ while Si-3s orbitals make major contributions in LiRbSi₂O₅. Hence, we can state that the metallic oxide and the [SiO₄] tetrahedra are responsible for the band-gap of LiKSi₂O₅ while [SiO₄] tetrahedra charge the band-gap of LiRbSi₂O₅. And, the differences in PDOS around the

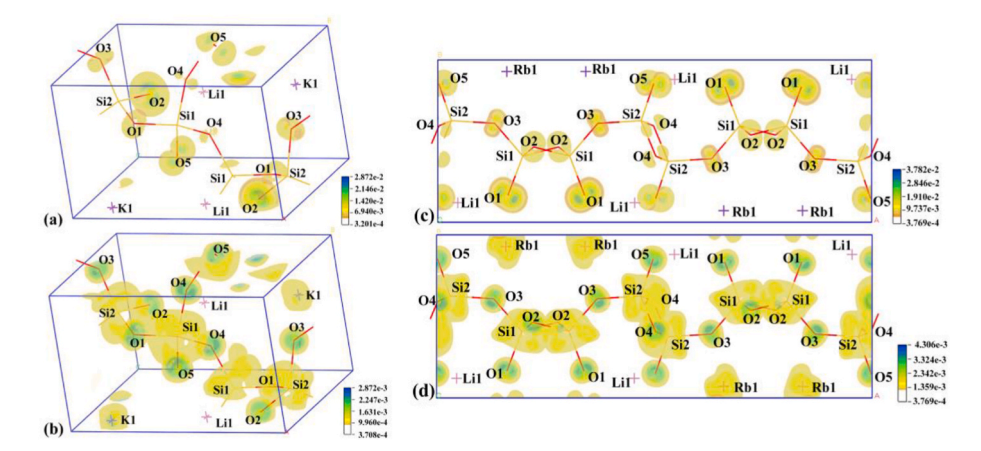


Fig. 4. The SHG density of occupied (a, c) and unoccupied (b, d) in LiKSi₂O₅ and LiRbSi₂O₅, respectively.

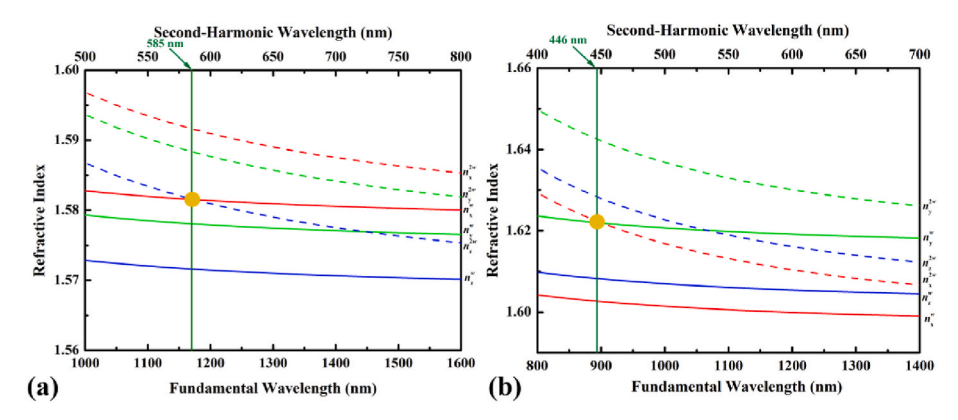


Fig. 5. Calculated refractive indices of the ordinary and extraordinary wavelengths for the fundamental (solid lines) and second-harmonic (dashed lines) wavelengths for LiKSi₂O₅ (a) and LiRbSi₂O₅ (b), respectively.

Fermi surface may relate to the catalytic activity of materials.

In addition, the SHG coefficients of the title compounds were also estimated by the first-principle calculations. Since LiKSi $_2$ O $_5$ belongs to 2 point group, it owns four nonzero independent SHG coefficients $d_{14} =$ 0.05 pm/V, $d_{16}=$ 0.30 pm/V, $d_{22}=$ 0.05 pm/V and $d_{23}=$ 0.02 pm/V based on Kleinman symmetry [56]. The calculated d_{16} , corresponding to $0.77 \times \text{KDP}$ (d_{36} (KDP) = 0.39 pm/V). For LiRbSi₂O₅, it has three nonzero independent SHG coefficients which belongs to mm2 point group, $d_{15} = 0.16$ pm/V, $d_{24} = 0.38$ pm/V, $d_{33} = 0.25$ pm/V. The calculated d_{24} corresponds to 0.97 \times KDP. To understand the source of SHG responses, the SHG densities [57,58] of the two compounds were plotted in Fig. 4. For LiASi₂O₅ (A = K, Rb), the virtual electron (VE) processes are analyzed because they have dominant contributions (>70 %) to the SHG effects compared with the virtual hole (VH). According to the results shown in Fig. 4, we found that the main contributions of occupied and unoccupied states are the O atoms, while the Si⁴⁺ and A⁺ atoms make little contributions. According to the anionic group theory [29], the cations' contributions to SHG are very small, so the total SHG responses are also very weak which explains why the small SHG responses of the two compounds have.

Apart from the SHG responses, the birefringence of the two compounds is also calculated. The birefringence is 0.010 at 1064 nm for LiKSi₂O₅, and 0.019 at 1064 nm for LiRbSi₂O₅, respectively (Figure S7) [17]. Hence, the shortest wavelengths of phase matching are calculated for LiASi₂O₅ (A = K, Rb) [17,59]. The calculated refractive indices as a function of wavelength are shown in Fig. 5. Again, the refractive indices at the fundamental (second-harmonic) wavelengths are shown as solid and dashed lines, respectively. And, the shortest wavelengths of phase matching occur at the first intersection of $n(\omega) = n(2\omega)$ [59,60]. In

Fig. 5, those occur when the solid red (green) line, $n(\omega)$, intersects with the dashed blue (red) line, $n(2\omega)$, respectively. The intersections are shown by orange circles and represented at 585 nm for LiKSi₂O₅, and 446 nm for LiRbSi₂O₅, respectively, which is fit well with the previous assumption.

4. Conclusions

In summary, two NLO silicates LiASi $_2O_5$ (A = K, Rb) have been synthesized by using the tetrahedral basic building units with differentiated symmetry and optical properties. LiKSi $_2O_5$ crystallizes in the monoclinic system of $P2_1$ (No. 4) while LiRbSi $_2O_5$ in the orthorhombic system of $Pca2_1$ (No. 29). The two compounds both have the short cutoff, 255 nm corresponding to 5.78 eV for LiKSi $_2O_5$, 240 nm corresponding to 5.94 eV for LiRbSi $_2O_5$, respectively. The SHG coefficients d_{ij} were calculated, the largest SHG coefficients $d_{16}=0.30$ pm/V in LiKSi $_2O_5$ corresponding to 0.77 \times KDP while $d_{24}=0.38$ pm/V in LiRbSi $_2O_5$ corresponding to 0.97 \times KDP. In addition, the shortest wavelengths of phase matching were also calculated, 585 and 446 nm for LiKSi $_2O_5$ and LiRbSi $_2O_5$, respectively. Accordingly, this paper provides an effective way to change the properties of the compounds by using the simple ion substitution.

CRediT authorship contribution statement

Jun Sun: Writing – review & editing, Writing – original draft, Visualization, Resources, Methodology, Investigation, Funding acquisition, Formal analysis, Data curation, Conceptualization. **Bo Ran:** Visualization, Resources, Investigation. **Ping Hu:** Visualization,

Investigation. **Zhaofeng Wu:** Writing – review & editing, Investigation, Funding acquisition. **Ming-Hsien Lee:** Writing – review & editing, Software, Investigation. **Haiming Duan:** Writing – review & editing, Visualization, Investigation.

Declaration of competing interest

The authors declare that they have no known competing financial interests or personal relationships that could have appeared to influence the work reported in this paper.

Data availability

No data was used for the research described in the article.

Acknowledgments

This work was financially supported by National Natural Science Foundation of China (Grand NO. 21964016), Natural Science Foundation of Xinjiang Uygur Autonomous (Grand NO. 2022D01C73), Tianshan Innovation Team Program of Xinjiang Uygur Autonomous Region (Grand NO. 2023D14001), and Tianchi Talent Program (Grand NO. TCBS202131).

Appendix A. Supplementary data

Supplementary data to this article can be found online at https://doi.org/10.1016/j.optmat.2023.114815.

References

- [1] P. Becker, Borate materials in nonlinear optics, Adv. Mater. 10 (1998) 979-992.
- [2] P.S. Halasyamani, K.R. Poeppelmeier, Noncentrosymmetric oxides, Chem. Mater. 10 (1998) 2753–2769.
- [3] M. Mutailipu, M. Zhang, B.B. Zhang, L.Y. Wang, Z.H. Yang, X. Zhou, S.L. Pan, SrB₅O₇F₃ functionalized with [B₅O₉F₃]⁶ chromophores: accelerating the rational design of deep-ultraviolet nonlinear optical materials, Angew. Chem. Int. Ed. 57 (2018) 6095–6099.
- [4] M. Mutailipu, F.M. Li, C.C. Jin, Z.H. Yang, K.R. Poeppelmeier, S.L. Pan, Strong nonlinearity induced by coaxial alignment of polar chain and dense [BO₃] units in CaZn₂(BO₃)₂, Angew. Chem. Int. Ed. 61 (2022) e202202096.
- [5] T.T. Tran, H.W. Yu, J.M. Rondinelli, K.R. Poeppelmeier, P.S. Halasyamani, Deep ultraviolet nonlinear optical materials, Chem. Mater. 28 (2016) 5238–5258.
- [6] B.B. Zhang, G.Q. Shi, Z.H. Yang, F.F. Zhang, S. L. Pan Fluorooxoborates, Beryllium-free deep-ultraviolet nonlinear optical materials without layered growth, Angew. Chem. Int. Ed. 56 (2017) 3916–3919.
- [7] Y.G. Shen, S.G. Zhao, Y. Yang, L.L. Cao, Z.J. Wang, B.Q. Zhao, Z.H. Sun, Z.S. Lin, J. H. Luo, A new KBBF-family nonlinear optical material with strong interlayer bonding, Cryst. Growth Des. 17 (2017) 4422–4427.
- [8] Z.Y. Zhou, Y. Qiu, F. Liang, L. Palatinus, M. Poupon, T. Yang, R.H. Cong, Z.S. Lin, J. L. Sun, CsSiB₃O₇: a beryllium-free deep-ultraviolet nonlinear optical material discovered by the combination of electron diffraction and first-principles calculations, Chem. Mater. 30 (2018) 2203–2207.
- [9] C.T. Chen, T. Sasaki, R.K. Li, Y.C. Wu, Z.S. Lin, Y. Mori, Z.G. Hu, J.Y. Wang, S. Uda, M. Yoshimura, Nonlinear Optical Borate Crystals: Principles and Applications, Wiley-VCH, Weinheim, 2012.
- [10] H.P. Wu, H.W. Yu, Z.H. Yang, X.L. Hou, X. Su, S.L. Pan, K.R. Poeppelmeier, J. M. Rondinelli, Designing a deep-ultraviolet nonlinear optical material with a large second harmonic generation response, J. Am. Chem. Soc. 135 (2013) 4215–4218.
- [11] T. Sasaki, Y. Mori, M. Yoshimura, Y.K. Yap, T. Kamimura, Recent development of nonlinear optical borate crystals: key materials for generation of visible and UV light, Math. Sci. Eng. R 30 (2000) 1–54.
- [12] E.L. Belokoneva, Borate crystal chemistry in terms of the extended OD theory: topology and symmetry analysis, Crystallogr. Rev. 11 (2005) 151–198.
- [13] H.T. Qiu, F.M. Li, Z. Li, Z.H. Yang, S.L. Pan, M. Mutailipu, Breaking the inherent interarrangement of [B₃O₆] clusters for nonlinear optics with orbital hybridization enhancement, J. Am. Chem. Soc. 145 (2023) 24401–24407.
- [14] D. Cyranoski, Materials science: China's crystal cache, Nature 457 (2009) 953-955.
- [15] T.Q. Sun, P. Shan, H. Chen, X.W. Liu, H.D. Liu, S.L. Chen, Y.a. Cao, Y.F. Kong, J. J. Xu, Growth and properties of a noncentrosymmetric polyphosphate CsLa(PO₃)₄ crystal with deep-ultraviolet transparency, CrystEngComm 16 (2014) 10497–10504.
- [16] S.G. Zhao, P.F. Gong, S.Y. Luo, L. Bai, Z.S. Lin, Y.Y. Tang, Y.L. Zhou, M.C. Hong, J. H. Luo, Tailored synthesis of a nonlinear optical phosphate with a short absorption edge, Angew. Chem. Int. Ed. 54 (2015) 4217–4221.

[17] M. Xia, F.M. Li, M. Mutailipu, S.J. Han, Z.H. Yang, S.L. Pan, Discovery of first magnesium fluorooxoborate with stable fluorine terminated framework for deep-UV nonlinear optical application, Angew. Chem. Int. Ed. 60 (2021) 14650–14656.

- [18] C.C. Jin, H. Zeng, F. Zhang, H.T. Qiu, Z.H. Yang, M. Mutailipu, S.L. Pan, Guanidinium fluorooxoborates as efficient metal-free short-wavelength nonlinear optical crystals, Chem. Mater. 34 (2022) 440–450.
- [19] C.T. Chen, B.C. Wu, A.D. Jiang, G.M. You, A new-type ultraviolet shg crystal β -BaB₂O₄, Sci. China, Ser. B 28 (1985) 235–243.
- [20] Y.N. Xia, C.T. Chen, D.Y. Tang, B.C. Wu, New nonlinear optical crystals for UV and VUV harmonic generation, Adv. Mater. 7 (1995) 79–81.
- [21] C.T. Chen, Y.C. Wu, A.D. Jiang, B.C. Wu, G.M. You, R.K. Li, S.J. Lin, New nonlinear-optical crystal: LiB₃O₅, J. Opt. Soc. Am. B 6 (1989) 616–621.
- [22] C.T. Chen, Y.B. Wang, B.C. Wu, K.C. Wu, W.L. Zeng, L.H. Yu, Design and synthesis of an ultraviolet-transparent nonlinear optical crystal Sr₂Be₂B₂O₇, Nature 373 (1995) 322–324.
- [23] H.P. Wu, S.L. Pan, K.R. Poeppelmeier, H.Y. Li, D.Z. Jia, Z.H. Chen, X.Y. Fan, Y. Yang, J.M. Rondinelli, H. Luo, K₃B₆O₁₀Cl: a new structure analogous to perovskite with a large second harmonic generation response and deep UV absorption edge, J. Am. Chem. Soc. 133 (2011) 7786–7790.
- [24] P. Yu, L.M. Wu, L.J. Zhou, L. Chen, Deep-ultraviolet nonlinear optical crystals: Ba₃P₃O₁₀X (X = Cl, Br), J. Am. Chem. Soc. 136 (2014) 480–487.
- [25] L. Li, Y. Wang, B.H. Lei, S.J. Han, Z.H. Yang, K.R. Poeppelmeier, S.L. Pan, A new deep-ultraviolet transparent orthophosphate LiCs₂PO₄ with large second harmonic generation response, J. Am. Chem. Soc. 138 (2016) 9101–9104.
- [26] Y.G. Shen, Y. Yang, S.G. Zhao, B.Q. Zhao, Z.S. Lin, C.M. Ji, L. Li, P. Fu, M.C. Hong, J.H. Luo, Deep-ultraviolet transparent Cs₂LiPO₄ exhibits an unprecedented second harmonic generation, Chem. Mater. 28 (2016) 7110–7116.
- [27] G. Peng, N. Ye, Z.S. Lin, L. Kang, S.L. Pan, M. Zhang, C.S. Lin, X.F. Long, M. Luo, Y. Chen, Y.H. Tang, F. Xu, T. Yan, NH₄Be₂BO₃F₂ and γ-Be₂BO₃F: overcoming the layering habit in KBe₂BO₃F₂ for the next-generation deep-ultraviolet nonlinear optical materials, Angew. Chem. Int. Ed. 57 (2018) 8968–8972.
- [28] M. Mutailipu, J. Han, Z. Li, F.M. Li, J.J. Li, F.F. Zhang, X.F. Long, Z.H. Yang, S. L. Pan, Achieving the full-wavelength phase-matching for efficient nonlinear optical frequency conversion in C(NH₂)₃BF₄, Nat. Photonics 17 (2023) 694–701.
- [29] C.T. Chen, G.Z. Liu, Recent advances in nonlinear optical and electro-optical materials. Annu. Rev. Mater. Sci. 16 (1986) 203–243.
- [30] C.T. Chen, Y.C. Wu, R.K. Li, The anionic group theory of the non-linear optical effect and its applications in the development of new high-quality nlo crystals in the borate series, Int. Rev. Phys. Chem. 8 (1989) 65–91.
- [31] C.T. Chen, Z. Lin, Z. Wang, The development of new borate-based UV nonlinear optical crystals, Appl. Phys. B 80 (2005) 1–25.
- [32] T.L. Chao, W.J. Chang, S.H. Wen, Y.Q. Lin, B.C. Chang, K.H. Lii, Titanosilicates with strong phase-matched second harmonic generation responses, J. Am. Chem. Soc. 138 (2016) 9061–9064.
- [33] H.P. Wu, B.B. Zhang, H.W. Yu, Z.G. Hu, J.Y. Wang, Y.C. Wu, P.S. Halasyamani, Designing silicates as deep-UV nonlinear optical (NLO) materials using edgesharing tetrahedra, Angew. Chem. Int. Ed. 59 (2020) 8922–8926.
- [34] S.T. Jiang, J.J. Zhou, H.P. Wu, H.W. Yu, Z.G. Hu, J.Y. Wang, Y. C. Wu PbSrSiO, A new ultraviolet nonlinear optical material with a strong second harmonic generation response and moderate birefringence, Chem. Commun. 56 (2020) 7104–7107.
- [35] J.J. Zhang, R.Q. Wei, D.Q. Yang, Y. Wang, B.B. Zhang, Searching for silicate nonlinear optical materials by combining calculation and experiment, Inorg. Chem. Front. 10 (2023) 4711–4718.
- [36] C.S. Lee, S.L. Wang, K.H. Lii, $Cs_2k(uo)_2si_4o_{12}$: a mixed-valence uranium (IV, V) silicate, J. Am. Chem. Soc. 131 (2009) 15116–15117.
- [37] C.C. Heyward, C.D. McMillen, J.W. Kolis, Hydrothermal growth of lanthanide borosilicates: a useful approach to new acentric crystals including a derivative of cappelenite, Inorg. Chem. 54 (2015) 905–913.
- [38] B.Q. Zhao, Y. Yang, S.G. Zhao, Y.G. Shen, X.F. Li, L.N. Li, C.M. Ji, Z.S. Lin, J.H. Luo, A new phase-matchable nonlinear optical silicate: Rb₂ZnSi₃O₈, J. Mater. Chem. C 5 (2017) 11025–11029.
- [39] J.J. Xu, H.P. Wu, H.W. Yu, Z.G. Hu, J.Y. Wang, Y.C. Wu, Syntheses, characterization and calculations of $Li_mA_nM_6O_{15}$ (A = Rb, Cs; M = Si, Ge; m + n = 6), Sci. China Mater. 63 (2020) 1769–1778.
- [40] B.H.W.S. D. Jong, H.T.J. Super, A.L. Spek, N. Veldman, W.V. Wezel, V. V. D. M, Structure of $\rm KLiSi_2O_5$ and the hygroscopicity of glassy mixed alkali disilicates, Acta Crystallogr. B52 (1996) 770–776.
- [41] Z. Du, N.H. de Leeuw, R. Grau Crespo, P.B. Wilson, J.P. Brodholt, M. Calleja, M. T. Dove, A computational study of the effect of Li-K solid solutions on the structures and stabilities of layered silicate materials-an application of the use of condor pools in molecular simulation, Mol. Simulat. 31 (2005) 339–347.
- [42] Z.M. Du, N.H. de Leeuw, The size effect of alkali ions on structural variations in layered silicate materials, J. Mater. Chem. 15 (2005) 4167–4178.
- [43] V.A. Saint, Bruker Analytical X-Ray Instruments, 2008. Madison, wi.
- [44] G.M. Sheldrick, Shelxtl Version 6.14, Bruker Analytical Xray Instruments, Madison, WI. 2003.
- [45] A. Spek, Single-crystal structure validation with the program platon, J. Appl. Crystallogr. 36 (2003) 7–13.
- [46] S.J. Clark, M.D. Segall, C.J. Pickard, P.J. Hasnip, M.I.J. Probert, K. Refson, M. C. Payne, First principles methods using castep, Z. für Kristallogr. Cryst. Mater. 220 (2005) 567–570.
- [47] B.G. Pfrommer, M. Côté, S.G. Louie, M.L. Cohen, Relaxation of crystals with the quasi-Newton method, J. Comput. Phys. 131 (1997) 233–240.
- [48] A.M. Rappe, K.M. Rabe, E. Kaxiras, J.D. Joannopoulos, Optimized pseudopotentials, Phys. Rev. B 41 (1990) 1227–1230.

- [49] J.S. Lin, A. Qteish, M.C. Payne, V. Heine, Optimized and transferable nonlocal separable ab initio pseudopotentials, Phys. Rev. B 47 (1993) 4174–4180.
- [50] L. Kang, D.M. Ramo, Z. Lin, P.D. Bristowe, J.G. Qin, C.T. Chen, First principles selection and design of mid-IR nonlinear optical halide crystals, J. Mater. Chem. C 1 (2013) 7363–7370.
- [51] J. Lin, M.H. Lee, Z.P. Liu, C. Chen, C.J. Pickard, Mechanism for linear and nonlinear optical effects in β -BaB $_2$ O $_4$ crystals, Phys. Rev. B 60 (1999) 13380–13389.
- [52] C. Aversa, J.E. Sipe, Nonlinear optical susceptibilities of semiconductors: results with a length-gauge analysis, Phys. Rev. B 52 (1995) 14636–14645.
- [53] W.W. Zhao, F.Y. Zhang, J. Liu, B. Hao, S.L. Pan, F.F. Zhang, L. Liu, Flux crystal growth of Ba₂TiOSi₂O₇, J. Cryst. Growth 413 (2015) 46–50.
- [54] M. Mutailipu, Z. Li, M. Zhang, D.W. Hou, Z.H. Yang, B.B. Zhang, H.P. Wu, S.L. Pan, The mechanism of large second harmonic generation enhancement activated by Zn²⁺ substitution, Phys. Chem. Chem. Phys. 18 (2016) 32931–32936.
- [55] P. Mori Sánchez, A.J. Cohen, W.T. Yang, Localization and delocalization errors in density functional theory and implications for band-gap prediction, Phys. Rev. Lett. 100 (2008) 146401.
- [56] D.A. Kleinman, Nonlinear dielectric polarization in optical media, Phys. Rev. 126 (1962) 1977–1979.
- [57] M.H. Lee, C.h. Yang, J.H. Jan, Band-resolved analysis of nonlinear optical properties of crystalline and molecular materials, Phys. Rev. B 70 (2004) 235110.
- [58] C.H. Lo, The Role of Electron Lone-Pair in the Optical Nonlinearity of Oxide, Tamkang University, 2005.
- [59] W.G. Zhang, H.W. Yu, H.P. Wu, P.S. Halasyamani, Phase-matching in nonlinear optical compounds: a materials perspective, Chem. Mater. 29 (2017) 2655–2668.
- [60] A. Ashkin, G.D. Boyd, D.A. Kleinman, Phase-matched second-harmonic generation in KDP without double refraction, Appl. Phys. Lett. 6 (1965) 179–180.